

EVALUATION OF SIMPLIFIED LOADING MODELS FOR FINITE ELEMENT ANALYSIS OF COMPOSITE WIND TURBINE BLADES

Rosemary H. Barnes¹, Evgeny V. Morozov, Krishna Shankar

School of Engineering and Information Technology, University of New South Wales at the Australian Defence Force Academy, Canberra, Australia

¹Email: rosemary.barnes@student.adfa.edu.au

Keywords: composite materials, loading, optimisation, finite element method, wind turbine blades

ABSTRACT

Wind turbine blades are large composite structures with complex geometry, and are subjected to non-uniform pressure distributions. These factors tend to make modelling and analysis laborious and computationally expensive. Simplified loading approximations are commonly used in wind turbine blade analysis, in place of accurate 3D pressure distributions to reduce modelling time and computational requirements. A review of twenty recent wind turbine blade design and analysis studies found that a wide variety of loading approximations were used, however very little has been published regarding the effect these approximations have on the accuracy of predicted structural behaviour. A comparison was performed of three of the most common loading approximations used in the reviewed literature: 3D pressure distribution derived from computational fluid dynamics; uniform pressure load derived from a blade element momentum (BEM) model; and a single tip force derived from BEM and beam theory. A finite element model of a 30m wind turbine blade was analysed under each of the loading approximations, and topological optimisation of the blade structure was performed using each of the approximations. Deflection, stress and failure criteria results were compared. Large discrepancies between the models were observed, particularly for stress distribution and tip rotation. The CFD loading approximation predicted the failure location near the maximum chord location, with a safety factor of 1.55. The uniform pressure approximation predicted failure at the same location and with similar deflection as the CFD approximation, but with a higher safety factor of 1.69. The tip load approximation predicted failure near the blade tip with a lower safety factor of 1.39. It also overestimated deflection by 74% and underestimated tip rotation by 58% compared to the CFD pressure distribution. The topological optimisation results for the tip load approximation were very different to the other approximations, with more material located at the blade tip. The results indicate that the choice of loading approximation has the potential to significantly affect the outcome of wind turbine blade design. In particular, using a tip force approximation even early in the structural design process is likely to lead to a very different topology and higher material usage than if a more realistic load approximation method is used.

1 INTRODUCTION

The aim of wind turbine blade structural design is typically to minimise the cost or weight of the blade, subject to a number of structural constraints. Finite element analysis enables a designer to represent the geometry and materials properties of a wind turbine blade with sufficient accuracy that the number of prototypes required for physical testing is greatly reduced. Another advantage of FEA is that mathematical optimisation algorithms can easily be applied to the design problem, a technique which forms the basis of many recent studies [1-11].

Modern wind turbine blades are up to 85m long, and consist of varying composite materials layouts throughout the structure. They are subject to a variety of aerodynamic loading cases, with complex associated pressure distributions that can be accurately calculated using computational fluid dynamics (CFD). The large physical size and complex aerodynamic loads result in large computational requirements for numerical models of wind turbine blades. This is of particular concern in structural

optimisation, as the model is analysed thousands of times through the course of the optimisation. One way to reduce the size of the numerical model is to approximate the loads that are applied to the blade structure. This occurs in full-scale testing for certification standards [12] and in academic literature. Although it is common practice to use loading approximations in wind turbine blade design and analysis, very little has been published regarding the accuracy and applicability of the various types of loading approximations used. Knill [13] compared stress results of a wind turbine blade structural model when the load was applied via a nodal pressure distribution versus the load applied via rigid link elements. Local stresses were found to be inaccurate with the rigid link model, although global results were similar. Joncas *et al* [4] performed a topology optimisation of a wind turbine blade segment using three different loading approximations: tip force, moment and constant pressure as well as combined loading. The topologies that resulted varied across the different modelling assumptions, suggesting that the loading approximation selected is an important factor in structural optimisation.

The aim of this work is to investigate the effect that loading approximation has on deflection, stress and failure criterion results. Three loading approximation methods were formulated, derived from a review of twenty recent (published 2004-2015) wind turbine blade design or analysis studies that used the finite element method.

The method used to apply the aerodynamic forces associated with the maximum gust loading case to the finite element model varied considerably amongst the literature reviewed. The most common approach was to apply one or a small number of point forces or moments to the blade (12 out of 20 [2-6, 10, 14-21]). Others applied a uniform pressure load (3 out of 20 [7, 8, 22]) or distributed pressure load (5 out of 20). Of the distributed pressure models, 3 varied in the spanwise direction only [1, 9, 23], with constant pressure across the chordwise direction and 2 varied in both the spanwise and edgewise directions: Knill [13] and Grujicic [24] used third party aerodynamics codes to calculate 2D pressure distributions at a number of spanwise stations and interpolated between them to obtain 3D pressure distributions.

2 MODEL DESCRIPTION

The blade design used in this work, illustrated in Figure 1, is adapted from a 30m blade from a 1.5MW wind turbine blade presented in [25]. The blade is made of glass fibre reinforced polymer (GFRP), with sandwich sections in the shear webs of the structural spar and trailing edge panels. The blade's geometry is representative of commercial designs, blending from a circular cross section at the blade root to a thickened S818 aerofoil at 25% span ($l/l_0=0.25$, where l is the spanwise location and l_0 is the blade length, as shown in Figure 1b). The thickness, chord, twist and spar location vary along the span, as presented in Table 1.

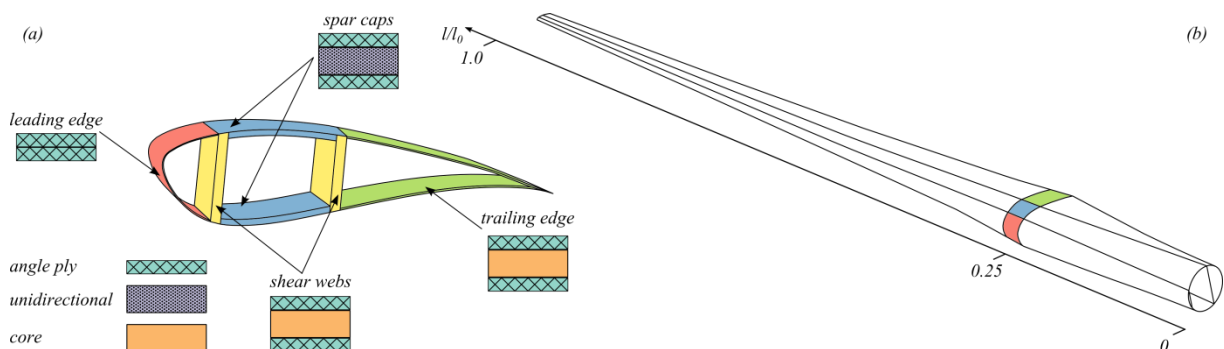


Figure 1: Blade design: a – materials placement; b - geometry

Span	Chord, m	Thickness	Twist	Aerofoil	Spar location
0%	1.56	100%	29.5°	Circle	10-60%
25%	2.58	28%	13.0°	S818	15-45%
35%	2.28	24%	8.8°	S818	15-45%
55%	1.71	22%	4.4°	S818	15-45%
75%	1.2	20%	1.9°	S818	15-45%
100%	0.6	18%	0°	S818	15-45%

Table 1: Baseline blade geometry

2.1 Finite Element Model

A finite element model of the blade has been created in ANSYS [26] using Shell281 elements, a layered shell element based on first-order shear deformation theory. Quadrilateral elements are used with corner and midside nodes and 6 degrees of freedom at each node and 0.05m element length. The blade is modelled with the root constrained and the tip free. The analyses are static and linear. Figure 2 shows the finite element model global (a) and element and fibre (b) coordinate systems.

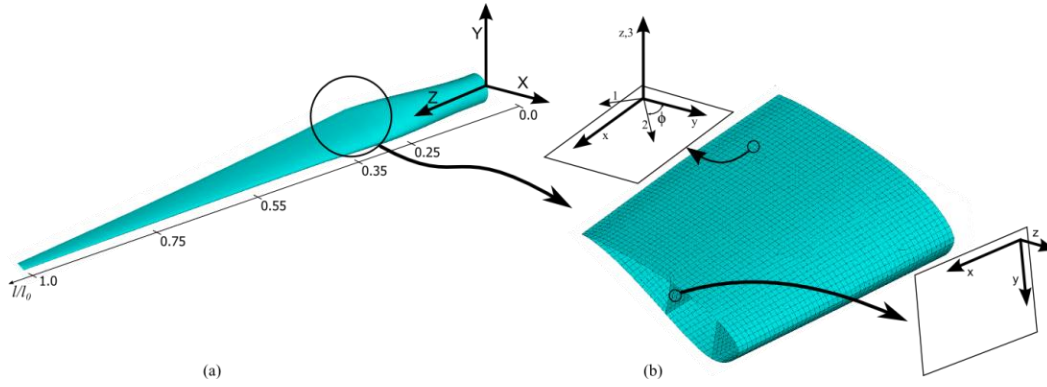


Figure 2: FE model coordinate systems: a – global, b – local

2.2 Materials

The blade structure has four different layouts, as illustrated in Figure 1a. The leading edge section is comprised of two 1.5mm thick GFRP fabric layers. The spar caps consist of a unidirectional layer (thicknesses listed in Table 2) aligned with the longitudinal axis between two 1.5mm thick GFRP fabric skins. The shear webs and trailing edge are sandwich panels with a lightweight core (thicknesses listed in Table 2) and GFRP fabric skins. Materials properties are given in Table 3 (sandwich core) and Table 4 (GFRP). The GFRP fabric is oriented with fibre angle, $\phi = 45^\circ$ in all cases. Material layer thickness is varied linearly between the values in Table 2 at 1.5m intervals.

Unidirectional layer, mm	Trailing edge core, mm	Shear web core, mm
22.1	10.1	30.3
39.3	7.46	22.4
39.3	4.73	14.2
32.5	3.17	9.51
17.5	1.88	5.64
9.2	1.88	5.64

Table 2: layer thicknesses

Property	Core
E Longitudinal modulus, GPa	0.13
G Shear modulus, GPa	0.035
$\bar{\sigma}_t$ Tensile strength, MPa	3.5
$\bar{\sigma}_c$ Compressive strength, MPa	2
$\bar{\tau}$ Shear strength, MPa	1.6
ρ Density, kg/m ³	100

Table 3: Core material properties

Property	GFRP fabric	GFRP unidirectional
E_1 Longitudinal modulus, GPa	25	39
E_2 Transverse modulus, GPa	25	8.3
G_{12} Shear modulus, GPa	6.3	4.1
ν_{12} Poisson's ratio	0.38	0.26
$\bar{\sigma}_{1t}$ Tensile strength, MPa	511	1062
$\bar{\sigma}_{1c}$ Compressive strength, MPa	628	610
$\bar{\sigma}_{2t}$ Tensile strength, MPa	511	31
$\bar{\sigma}_{2c}$ Compressive strength, MPa	628	118
$\bar{\tau}_{12}$ In-plane shear strength, MPa	790	72
ρ Density, kg/m ³	1900	1900

Table 4: GFRP properties

3 LOADING APPROXIMATIONS

The loading case considered in this work is extreme aerodynamic loading, defined as the maximum gust wind speed expected in a 50 year period, as specified in the IEC design requirements [1]. This was the most common loading case used in the reviewed literature (16 out of 20). Under this condition, the turbine is parked, and the blade under consideration is vertical in the uppermost position, illustrated in Figure 3. For a Class I site the maximum gust wind speed is 70 m/s at the hub height, and due to wind shear the wind speed increases above that height according to:

$$v/v_o = (h/h_o)^{0.14} \quad (1)$$

Where v is velocity, h , is height above ground, the subscript 'o' is the reference height, in this case the hub height, and the exponent 0.14 is the wind shear exponent specified in the IEC requirements.

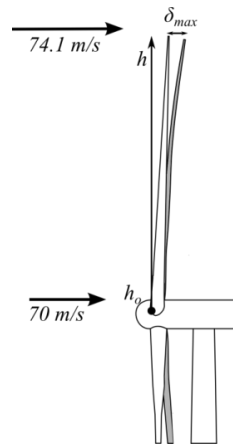


Figure 3: Maximum gust loading condition with wind shear

The maximum gust loading condition was applied to the finite element structural model using three different methods of approximation, outlined in the following sections.

3.1 Computational fluid dynamics

The external surface from the blade FEA model was used to create a CFD model of the airflow around the blade. A finite volume method was employed to solve 3D, viscous, compressible Navier Stokes equations with the k-omega SST turbulence model in ANSYS Fluent [27]. A cylindrical fluid volume was analysed, with diameter 90m from 30m upstream to 60m downstream of the blade. The blade surface mesh was refined with face sizing of 0.1m, and ten inflation layers. The entire CFD model consisted of 853,986 cells. Wind shear was incorporated using a linear interpolation between the wind speed at hub height (70m/s) and at the blade tip (74.1m/s).

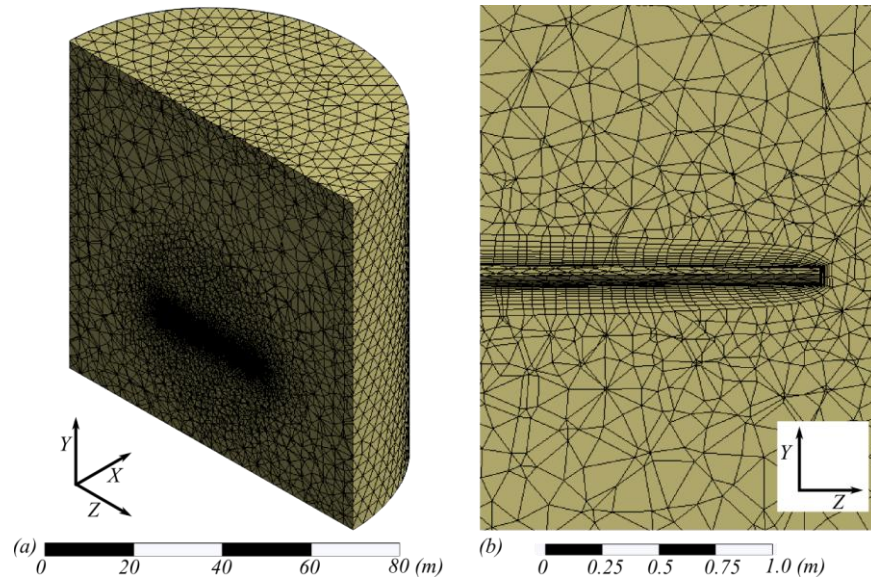


Figure 4: CDF mesh: a - entire model cross section; b - blade tip area

The resulting pressure distribution has relatively uniform large magnitude positive pressure across the upwind side of the blade, and very small magnitude negative pressure across the downwind side. There are localised areas of large negative pressure at the leading and trailing edge of the blade, particularly the near-cylindrical portion of the blade root. The total pressure force components summed over the entire blade surface are given in Table 5. The CFD pressure distribution at the blade surface was exported to ANSYS APDL and translated to a series of nodal pressures to match the FEA mesh. Figure 5 shows the CFD pressure distribution as applied to the FEA model. The colour scale shows the absolute value of nodal pressure.

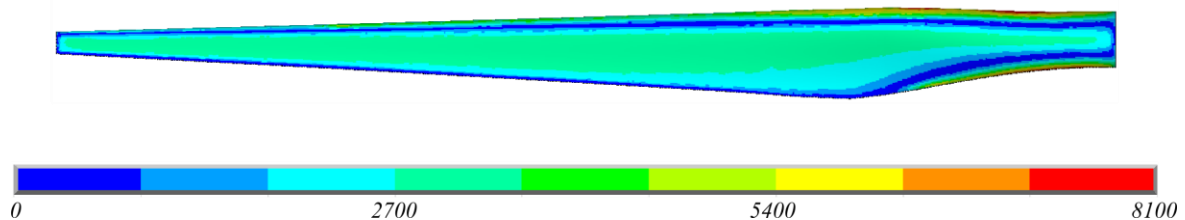


Figure 5: CFD pressure distribution as applied to FE model (upwind side)

Direction	Total force
X	63,518 N
Y	163,658 N
Z	-5,908 N
Resultant	175651 N

Table 5: CFD force breakdown

3.2 Uniform pressure load

The second loading approximation applied the total drag force as a uniform pressure load on one side of the blade, as shown in Figure 6. The magnitude of the drag force was calculated using a blade element momentum (BEM) model. The BEM model splits the wind turbine blade into 20 spanwise elements. The drag force is calculated for each element, using local wind velocities that vary due to wind shear (Eq. 1) and assuming a flat plate drag coefficient, C_D , of 1.2 from 10% to 90% span, with

reduced drag coefficients at the root and tip. The total drag force determined by the BEM model was 184,338N, which correlates well to the total force obtained using the CFD model. The magnitude of the uniform pressure applied was obtained by dividing the total drag force by the planform area, resulting in a pressure load of 3,727 N/m² which was applied to the upwind side of the blade.



Figure 6: Uniform pressure load approximation (upwind side)

Span, m	Chord, m	Velocity, m/s	C _D	Force, N
0	1.56	70.0	0.8	
1.5	1.56	70.2	0.8	5,657
3.0	1.95	70.5	1.2	10,679
4.5	2.34	70.7	1.2	12,900
6.0	2.46	70.9	1.2	13,649
7.5	2.58	71.2	1.2	14,405
9.0	2.43	71.4	1.2	13,651
10.5	2.28	71.6	1.2	12,886
12.0	2.13	71.8	1.2	12,109
13.5	1.98	72.0	1.2	11,322
15.0	1.85	72.2	1.2	10,610
16.5	1.71	72.4	1.2	9,888
18.0	1.59	72.6	1.2	9,244
19.5	1.47	72.8	1.2	8,592
21.0	1.34	73.0	1.2	7,844
22.5	1.20	73.2	1.2	7,087
24.0	1.08	73.4	1.2	6,411
25.5	0.96	73.6	1.2	5,727
27.0	0.84	73.7	1.2	5,035
28.5	0.72	73.9	1.0	3,614
30.0	0.6	74.1	1.0	3,026
				184,338

Table 6: Blade element momentum model

3.3 Point load

The magnitude and location of the force applied in the point load approximation should be selected to yield results that are as similar to the real load as possible. Due to the complex geometry and materials of the wind turbine blade, determining what that load should be is not a trivial task. A typical approach to convert a distributed load to an equivalent point load is to apply the full magnitude of the distributed load at the centroid of the load area, in this case at approximately 40% span. This was the approach taken in the blade section analyses in [17, 18], and also in full-scale testing. With this approach, however, the behaviour of the blade outboard of this point cannot be accurately reflected. This is appropriate if only the section inboard of the applied load is being considered, as was the case in [17]. However, if the entire blade structure is of interest applying the load at the blade tip is considered more appropriate and was consequently the approach taken in this work.

The method used to determine the magnitude of the force applied at the blade tip was based on beam theory formulations for deflection of a cantilever beam. The load distribution and bending moment distribution for the BEM model (blue, solid), linear tapered load (red, dotted) and uniform

load (green, dashed) are shown in Figure 7. In all cases the total load is the same: for the uniform load, the distributed load $\omega = D/l$, where D is the total drag force from the BEM model; and for the linear tapered distribution, $\omega = \frac{\omega_0}{l}(l - x) \rightarrow \omega_0 = 2D/l$. Based on the load and bending moment distributions, the linear tapered distributed load was selected as a reasonable approximation of the BEM load distribution.

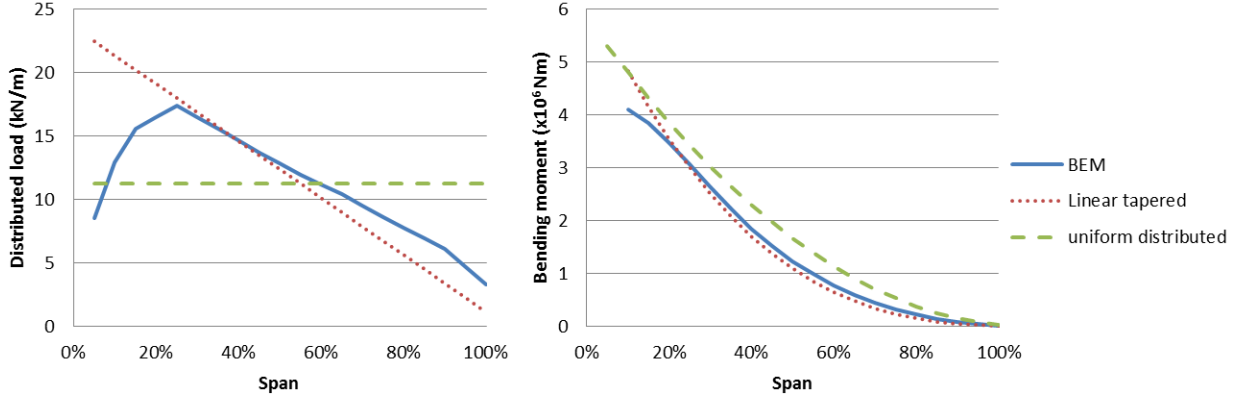


Figure 7: simplified load comparisons: a – distributed load; b – bending moment

For a cantilever beam of length l with a concentrated load, P , at the free end, the maximum deflection is given by:

$$\delta_{max} = \frac{Pl^3}{3EI} \quad (2)$$

Where E is Young's modulus and I is the moment of inertia.

For a linear tapered distributed load, the maximum deflection is:

$$\delta_{max} = \frac{\omega_0 l^4}{30EI} \quad (3)$$

Combining (2) and (3):

$$\begin{aligned} \frac{Pl^3}{3EI} &= \frac{\omega_0 l^4}{30EI} \\ \therefore P &= \frac{D}{5} \end{aligned} \quad (4)$$

The single load approximation therefore consisted of a 36,868N force applied at the blade tip. The blade tip is a rigid region, with all nodes located at the tip constrained to a master node in the centre, as shown in Figure 8. The force, P , was applied to the master node.

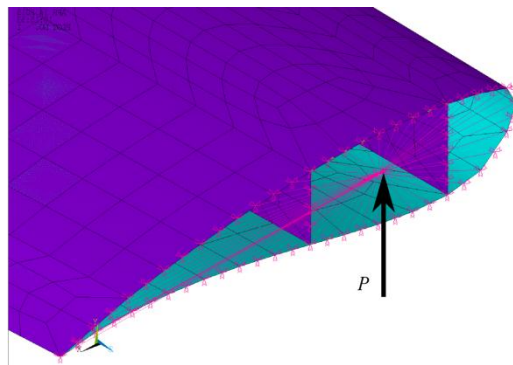


Figure 8: Point load approximation: tip nodes are a rigid region with force, P , applied to master node

4 LOADING APPROXIMATION COMPARISON

The finite element model described in Section 2 was analysed using each of the loading approximations in turn. Deflection, stress and failure criteria results were calculated, and are presented in Table 7. For each of the loading approximations, the magnitude was increased until the maximum failure criterion exceeded 1, in order to determine the failure location and safety factor associated with each loading approximation. For the uniform pressure and point load approximations, this was achieved by a simple scaling of the load magnitude. This method is not appropriate for the CFD approximation, so in this case the wind speed was increased and the CFD model rerun to get the new pressure distribution. The total resultant load at failure for the CFD approximation was 1.55 times the original load, corresponding to a 26% increase in wind speed.

Loading approximation		Applied load	Tip deflection	Tip rotation	max σ_{1c} value	max σ_{1c} location	Safety factor	Failure location
			m	°	MPa	m		m
1	CFD	175,651 N	3.23	4.88	140.7	7.5	1.55	7.5
2	Uniform	3,727 Pa	3.23	4.09	174.7	0.7	1.69	7.5
3	Point	36,868 N	5.62	2.04	384.9	25.6	1.39	25.6
3b	Point	23,042 N	3.50	1.27	242.5	25.6		

Table 7: Structural analysis results

Tip deflection is measured as the Y-component nodal displacement of the tip node. Tip rotation is defined as shown in Figure 9.

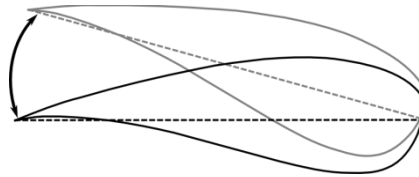


Figure 9: Tip rotation definition

The maximum compressive stress in the fibre direction is designated max σ_{1c} . In all cases this occurs in the unidirectional layer of the spar cap on the downwind side of the blade. The spanwise location for each model is also recorded. The failure criterion used is the Tsai-Wu criterion as implemented in ANSYS.

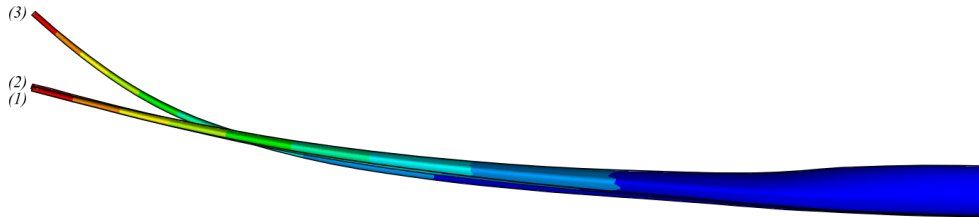


Figure 10: Deformed models: 1 – CFD; 2 – uniform pressure; 3 – point load

The deformed structures are shown in Figure 10. The maximum deflection of the CFD loading approximation (1) and uniform pressure approximation (2) are very close, but the point load approximation (3) is 74% higher. Due to the large discrepancy, a second variant of the tip load approximation was analysed, with a load magnitude of 23,042N (12.5% of the BEM force instead of 20% in the original point load model). This approximation (3b) in Table 7, has a tip deflection closer (8% larger) to that of approximations 1 and 2.

There is a large variation in the tip rotation results throughout the loading approximations. The twist predicted by approximation 2 is 16% less than that of 1 and the point load approximations 3 and 3b are less than half the value of 1. This is not surprising, as neither the uniform pressure load or point load approximations accurately represent the chordwise variation of the pressure distribution. Tip rotation is not necessarily relevant to the maximum gust loading condition investigated here, but would need to be accounted for if an operational loading condition is being considered, as excessive twisting would compromise aerodynamic performance.

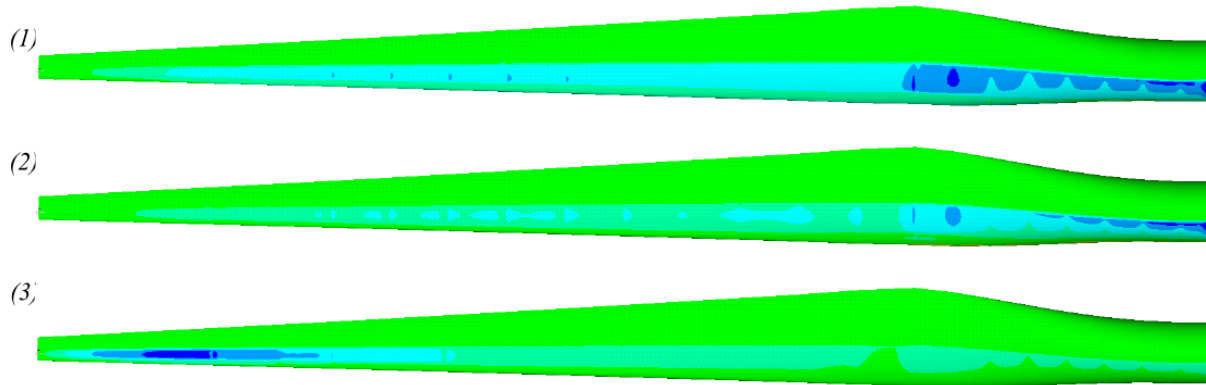


Figure 11: σ_{1c} Stress distribution: 1 – CFD; 2 – uniform pressure; 3 – point load

Figure 11 shows the stress distribution for each approximation. Dark blue corresponds to higher compressive stress; green corresponds to lower compressive stress. Note that the scale is not the same between the 3 approximations. The stress distributions are qualitatively fairly similar between approximations 1 and 2, with approximation 1 showing a slightly more even stress distribution along the span compared to approximation 2, which shows greater stress concentration at the blade root, and indeed this is the location of maximum stress for this approximation, whereas it is located near the maximum chord ($l/l_0=0.25$) in approximation 1. The stress distribution of approximation 3 is very different to the other two, with stresses concentrated at the blade tip. The maximum compressive stress values differ significantly between the models. Approximation 2 has maximum compressive stress 24% higher than the result from approximation 1, and the point load approximations 3 and 3b were higher again, with maximum compressive stress values 173% and 72% greater, respectively, than approximation 1.

The Tsai-Wu failure criterion distributions at failure load are shown in Figure 12. Compared to approximation 1, the safety factor of approximation 3 was underestimated and 2 was overestimated. The predicted failure location is the same in approximation 1 and 2, at the maximum chord location, but is located near the blade tip for approximation 3.

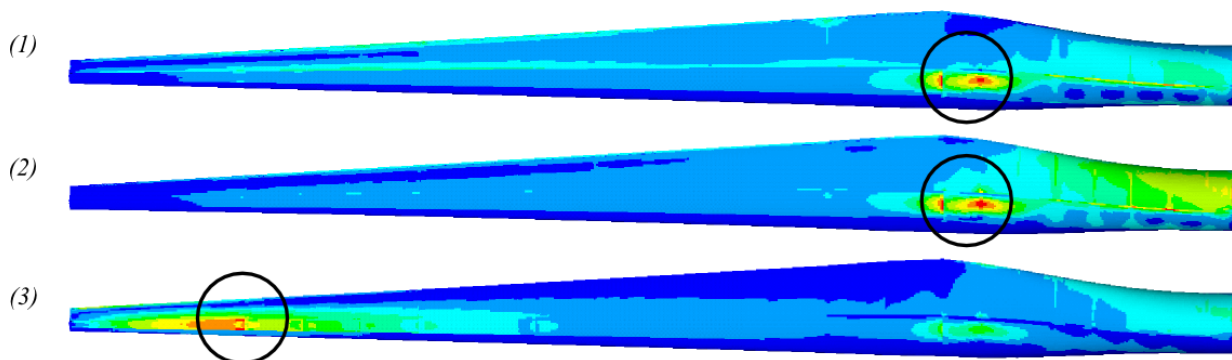


Figure 12: Tsai-Wu criterion distribution at failure load: 1 – CFD; 2 – uniform pressure; 3 – point load

5 STRUCTURAL OPTIMISATION

The results from the previous section indicate that loading approximation has the potential to significantly affect the structural behaviour of the blade. Deflection, stress and strength criteria are used as constraints early in the structural design process, which means that erroneous results in these areas have the potential to significantly affect the design process. Topological optimisation of the blade structure was performed with each loading approximation in order to investigate this further.

Wind turbine blades are particularly suited to topology optimisation as the asymmetrical structure and complex loading makes it difficult to intuitively obtain optimal layouts. The main advantage of topology optimisation is that it doesn't pre-define the configuration and so allows non-intuitive designs to result. Topology optimisation begins with the entire volume meshed with solid elements, and then determines where material should be placed within the volume to minimise the objective function. The design variables are the densities of every element of the interior volume, and the objective function is typically to minimise compliance (analogous to maximising stiffness) subject to a constraint on the proportion of volume to be removed. Penalty terms are used to try to ensure that elements have densities of either zero or 100% (corresponding to material absent or present, respectively).

5.1 Optimisation problem formulations

The topology optimisation feature in ANSYS 13.0 was used to create indicative structures for each of the loading models. The external blade geometry was maintained from the FEA model described in Section 2, but was meshed with solid tetrahedral elements throughout the entire interior blade volume, as well as shell elements on the exterior surfaces. In order to keep computational requirements moderate, the mesh density varied along the span. For the root section where the blade thickness is largest, an element length of 0.12m was used. The middle section had an element length of 0.06m, and the tip section where the blade thickness is smallest had an element length of 0.03m. The objective function of the optimisation was to minimise compliance, subject to a volume constraint of 25% (i.e. 75% of the volume was removed). The exterior shell elements were not part of the design domain but were present to allow surface loads to be transferred and to provide the structural function that is performed by the external shell. The result of the optimisation is a material distribution that shows where material is best placed to resist the applied loads. These results do not represent feasible designs, but simply yield insights into the load paths and the structural topologies that are best suited to the different loading models.



Table 8: Meshed model used for topology optimisation

5.2 Optimisation results

The topology optimisation results are shown in Figure 13. All three structures have a trailing edge spline, and spar caps that vary in width and chordwise location along the span. The point load structure has more material located at the tip than the other structures, which show spar caps that are very tapered at the tip. The CFD pressure distribution structure has a longer trailing edge spline than the uniform pressure distribution structure; although otherwise the structures are very similar. It should be noted that the mesh used in these optimisations is too coarse to allow subtle variations to show. For example, the spar caps in models 1 and 2 are a single layer of elements thick, which means it is not possible to draw any conclusions about the relative thickness and chordwise extent of the spar caps in these models. Sizing optimisation would be required to investigate this further. It is clear from the topology optimisations that the blade optimised for the tip load approximation is quite different to the

more accurate approximations. Using the tip load approximation even in preliminary design is likely to adversely affect the final blade design, likely resulting in increased material usage.



Figure 13: topology optimisation results: 1 – CFD; 2 – uniform pressure; 3 – point load

6 CONCLUSIONS

The results show significant discrepancies between the loading approximation methods for both deflection and stress results. The safety factor varied significantly between all three approximations, compared to the CFD approximation with a safety factor of 1.55 and failure predicted at the maximum chord location, the uniform pressure approximation had a higher predicted safety factor of 1.69 and the same predicted failure location, whereas the tip load approximation had a lower safety factor of 1.39 and predicted failure near the blade tip. The extent of tip rotation, 4.88° for the CFD approximation, was slightly underestimated by the uniform pressure distribution (4.09°), and much lower for the tip load approximations (2.04° and 1.27° for the larger and smaller point load approximations, respectively). This is not necessarily relevant to the maximum gust loading condition investigated here, but would need to be accounted for if an operational loading condition is being considered, as excessive twisting would compromise aerodynamic performance. Deflection was significantly overestimated by the point load approximation. Furthermore it was found that it was difficult to select an appropriate magnitude for the single force. The initial point load approximation had excessive tip deflection and maximum compressive stress results. The smaller of the two point load models was selected so as to result in reasonable tip deflection, which necessitated performing initial analysis with a more accurate loading model for comparison, somewhat reducing the benefit gained from using a simplified model in the first place. The smaller point load approximation still had maximum compressive stress 72% higher than the CFD approximation. The structure resulting from topology optimisation using the point load approximation was very different to the other approximation methods, demonstrating that even at the preliminary design level the point load approximation is likely to adversely affect the design process.

REFERENCES

1. Bottasso, C.L., et al., *Structural optimization of wind turbine rotor blades by multilevel sectional/multibody/3D-FEM analysis*. Multibody System Dynamics, 2014. **32**(1): p. 87-116.
2. Jureczko, M., M. Pawlak, and A. Mężyk, *Optimisation of wind turbine blades*. Journal of Materials Processing Technology, 2005. **167**(2–3): p. 463-471.
3. Forcier, L.-C. and S. Joncas, *Development of a structural optimization strategy for the design of next generation large thermoplastic wind turbine blades*. Structural and Multidisciplinary Optimization, 2011: p. 1-18.
4. Joncas, S., M.J. de Ruiter, and F.v. Keulen, *Preliminary Design of Large Wind Turbine Blades Using Layout Optimization Techniques*, in *10th AIAA/ISSMO Multidisciplinary Analysis and Optimization Conference 2004*, American Institute of Aeronautics and Astronautics: Albany, New York.
5. Lund, E. and J. Stegmann, *On structural optimization of composite shell structures using a discrete constitutive parametrization*. Wind Energy, 2005. **8**(1): p. 109-124.

6. Sørensen, S.N., R. Sørensen, and E. Lund, *DMTO – a method for Discrete Material and Thickness Optimization of laminated composite structures*. Structural and Multidisciplinary Optimization, 2014. **50**(1): p. 25-47.
7. Liu, W., et al. *A Kind of Innovative Design Methodology of Wind Turbine Blade Based on Natural Structure*. in *Information and Computing Science, 2009. ICIC '09. Second International Conference on*. 2009.
8. Buckney, N., et al., *On the structural topology of wind turbine blades*. Wind Energy, 2013. **16**(4): p. 545-560.
9. Hu, W., et al., *Multi-objective structural optimization of a HAWT composite blade based on ultimate limit state analysis*. Journal of Mechanical Science and Technology, 2012. **26**(1): p. 129-135.
10. Pirrera, A., et al., *Optimization of Wind Turbine Blade Spars*, in *53rd AIAA/ASME/ASCE/AHS/ASC Structures, Structural Dynamics and Materials Conference 2012*: Honolulu, Hawaii.
11. Lindgaard, E., E. Lund, and K. Rasmussen, *Nonlinear buckling optimization of composite structures considering “worst” shape imperfections*. International Journal of Solids and Structures, 2010. **47**(22–23): p. 3186-3202.
12. Commission, I.E., *Wind Turbines - Part 1: Design Requirements*, 2005: Geneva.
13. Knill, T.J., *The application of aeroelastic analysis output load distributions to finite element models of wind*. Wind Engineering, 2005. **29**(2): p. 153-168.
14. Branner, K., et al., *Torsional performance of wind turbine blades - Part II: Numerical Validation*, in *ICCM 16th International Congress on Composite Materials 2007*: Kyoto, Japan.
15. Cárdenas, D., et al., *Numerical validation of a finite element thin-walled beam model of a composite wind turbine blade*. Wind Energy, 2011.
16. Li, Z., et al., *Effect of Lay-up Design on Properties of Wind Turbine Blades*. Frontiers of Engineering Mechanics Research, 2013. **2**(3): p. 63-70.
17. Lindgaard, E. and E. Lund, *Nonlinear buckling optimization of composite structures*. Computer Methods in Applied Mechanics and Engineering, 2010. **199**(37–40): p. 2319-2330.
18. Overgaard, L.C.T., E. Lund, and O.T. Thomsen, *Structural collapse of a wind turbine blade. Part A: Static test and equivalent single layered models*. Composites Part A: Applied Science and Manufacturing, 2010. **41**(2): p. 257-270.
19. Wu, W.-H. and W.-B. Young, *Structural Analysis and Design of the Composite Wind Turbine Blade*. Applied Composite Materials: p. 1-11.
20. Singh, R.K., et al., *Design of a low Reynolds number airfoil for small horizontal axis wind turbines*. Renewable Energy, 2012. **42**: p. 66-76.
21. Wen-Bin, Y. and W. Wen-Hsiang. *Optimization of the skin thickness distribution in the composite wind turbine blade*. in *International Conference on Fluid Power and Mechatronics*. 2011.
22. Nugroho, I.H., et al., *Lay-up design of low wind speed composite turbine blade*. Key Engineering Materials, 2011. **471-472**: p. 981-986.
23. Berggreen, C., et al., *Application and analysis of sandwich elements in the primary structure of large wind turbine blades*. Journal of Sandwich Structures & Materials, 2007. **9**(6): p. 525-552.
24. Grujicic, M., et al., *Structural-Response Analysis, Fatigue-Life Prediction, and Material Selection for 1 MW Horizontal-Axis Wind-Turbine Blades*. Journal of Materials Engineering and Performance, 2010. **19**(6): p. 790-801.
25. Berry, D., et al., *Parametric study for large wind turbine blades*, 2002, Sandia.
26. ANSYS, I., *Theory Reference for the Mechanical APDL and Mechanical Applications*, 2009.
27. ANSYS, I., *ANSYS Fluent Theory Guide*, 2013.